Engineered Science

RESEARCH PAPER View Article Online

Heterogeneous Iridium Oxide/Gold Nanocluster for Non-enzymatic Glucose Sensing and pH Probing

Qiuchen Dong,[1*] Xudong Wang,[2] Haomin Liu,[3] Heejeong Ryu,[3] Jing Zhao,[2] Baikun Li[4] and Yu Lei[1,3*]

In this work, heterogeneous gold-doped iridium oxide nanoclusters (IrO_2–Au NCs) that are both pH-sensitive and glucose-responsive were synthesized through electrospinning followed by high-temperature calcination. The as-prepared IrO_2–Au NCs were systematically characterized using various advanced techniques including scanning electron microscopy, X-ray powder diffraction and Raman spectroscopy. They were then employed as the sensing element to fabricate a sensor for both non-enzymatic glucose sensing and solid-state pH monitoring. Sensing performance of the IrO_2–Au NCs based dual sensor toward pH and glucose was evaluated using various electrochemical techniques, including potentiometric, cyclic voltammetry and amperometric techniques. The results show that the as-prepared IrO_2–Au NCs not only maintain accurate and reversible pH sensitivity derived from IrO_2, but also demonstrate good electrocatalytic activity resulted from Au toward glucose oxidation in alkaline medium at a low applied potential with a sensitivity of 21.20 μA mM^{-1} cm^{-2}, a limit of detection of 2.93 μM (S/N=3) and a reasonable selectivity against various interferences. These features show that the as-prepared IrO_2–Au NCs hold great promise as a dual-functional sensing material for the development of a high-performance sensor for both solid-state pH and non-enzymatic glucose sensing.

Keywords: Iridium oxide-Au; Nanoclusters; Electrospinning; Non-enzymatic; Glucose detection; pH sensing; Dual sensor

Received 28 February 2019**, Accepted** 22 May 2019

DOI: 10.30919/es8d512

Introduction

In the past decades, both pH and glucose sensing technology have been separately and extensively studied due to their importance in probing the acidity/alkalinity of aqueous solutions and blood glucose level for diabetic patients, respectively. With respect to pH sensing, conventional glass-type pH electrode is the most widely used in laboratory environment; however, it suffers from the fragileness. Therefore, ion-selective field effect transistor[1-4] and optical pH sensors[5] are developed to improve the durability of pH sensors. However, their wider applications are greatly limited by its high power consumption, high cost, and unsuitability for harsh environment applications. Therefore, solid-state pH sensors that measure the electromotive force difference between the sensing and reference electrodes have gradually attracted researchers' attention in pH sensing because of their ability for miniaturization, cost-effectiveness, as well as the long-term stability and durability. Up to date, a spectrum of pH-responsive metal oxides have been extensively studied for pH detection,[6-7] some of which hold great promise. In regard to glucose sensing, intermittent and continuous glucose monitoring is of paramount importance for diabetic patients to track and manage their blood glucose level. Nowadays, glucose oxidase (GOx) and glucose dehydrogenase (GDH) based test strips dominate glucose sensor market. Although great success has been achieved using GOx and GDH, the intrinsic thermal and chemical sensitivity of enzyme stimulates the research community to pursuit more stable non-enzymatic catalysts in glucose detection. Consequently, non-enzymatic glucose sensors are developed as an alternative. Amongst various types of non-enzymatic glucose sensing materials, metal oxides stand out in the development of non-enzymatic glucose sensors because of their easy accessibility, low cost, and superior chemical/thermal stability. A range of metal oxides and their composite materials (e.g. Co_3O_4,[8-10] Co_3O_4/graphene,[11] NiO,[12] noble metal doped NiO,[13] CuO,[14-15] Cu_2O-TiO_2,[16] etc.) were exploited as innovative non-enzymatic glucose catalysts in glucose detection, respectively.

Although there are numerous reports about solid-state pH sensing or metal oxide based non-enzymatic glucose sensing, a majority of the techniques are developed based on the concept of "one sensor for one target". The development of dual sensors is heavily overlooked because of the lack of multi-functionality in a single sensing material. Therefore, a dual sensor, which can accomplish both non-enzymatic glucose sensing and solid-state pH sensing, still remains elusive. To accomplish dual sensor concept, novel functional sensing materials or current sensing materials with newly explored functions should be employed in the construction of sensors.

In our previous study,[17] iridium oxide has been demonstrated with both good solid-state pH sensing and glucose sensing properties, while noble metals, especially Au[18] and Pt,[19] show good conductivity and glucose sensing property. To further improve the sensing performance of iridium oxide, in this study, gold is doped into iridium oxide during its preparation process. Compared to pristine iridium oxide, gold-doped iridium oxide nanostructured material is expected to not only possess

[1] *Department of Biomedical Engineering, University of Connecticut, 191 Auditorium Rd, Storrs, CT, 06269-3222, USA*
[2] *Department of Chemistry, University of Connecticut, 55 N Eagleville Rd, Storrs, CT, 06269-3060, USA*
[3] *Department of Chemical and Biomolecular Engineering, University of Connecticut, 191 Auditorium Rd, Storrs, CT, 06269-3222, USA*
[4] *Department of Civil and Environmental Engineering, University of Connecticut, 261 Glenbrook Rd, 06269-3037, USA*
***E-mail:** qiuchen.dong@uconn.edu; yu.lei@uconn.edu*

pH sensing property inherited from iridium oxide, but also hold promise to lower the operating potential in glucose sensing which is attributed to gold.

The goal of this study aims at developing a dual functional electrochemical sensor for both glucose and pH sensing using a composite sensing material, which consists of IrO_2 and Au. Au-doped IrO_2 nanoclusters (IrO_2-Au NCs) were prepared by electrospinning followed by a high temperature annealing process. The as-prepared IrO_2-Au NCs was employed to modify glassy carbon electrode. Its pH and glucose sensing performance was systematically investigated using potentiometric, cyclic voltammetry and amperometric techniques.

2. Experimental

2.1 Reagents

Iridium (IV) tetrachloride ($IrCl_4$) was purchased from Alfa Aesar and used without further purification. Polyvinylpyrrolidone (PVP, MW=1,300,000) and Nafion 117 solution (purum, ~20% in a mixture of lower aliphatic alcohols and water) were supplied from Sigma-Aldrich. Hydrogen tetrachloroaurate trihydrate ($HAuCl_4 \cdot 3H_2O$) Dimethylformamide (DMF), D-(+)-glucose, 4-acetominopheon, ascorbic acid, and uric acid, as well as ethanol were obtained from Acros Organics. All aqueous solutions were prepared with deionized water (18.2 MΩ cm) generated by a Barnstead water system.

2.2 Fabrication of IrO_2-Au nanoclusters

For preparation of IrO_2-Au nanoclusters, 0.19 g iridium tetrachloride was dissolved in 4 mL of dimethylformamide (DMF) solution, followed by addition of 0.1 g $HAuCl_4$ and another 0.87 g PVP. The mixed solution was overnight stirred under magnetic stirring. The as-prepared homogenous solution was then electrospun using 23-gauge needle with a flow rate of 0.3 mL/h at an applied voltage of 20 kV over an aluminum foil collector (15 cm to the tip of needle). Such precursor solution without the addition of $HAuCl_4$ or $IrCl_4$ was also prepared for control experiments. The $IrCl_4$-$HAuCl_4$/PVP and $IrCl_4$/PVP nanofibers collected on the collector were then peeled off. After 3 h dehydration process at 80 °C in an oven, the as-prepared precursory $IrCl_4$-$HAuCl_4$/PVP or $IrCl_4$/PVP nanofibers were calcined under ambient atmosphere at 900 °C for 3 h with a ramp-up speed at 2 °C/min. The furnace was then allowed to naturally cool down to room temperature and the annealed IrO_2-Au NCs and IrO_2 NCs were collected.

2.3 Preparation of IrO_2-Au NCs modified glassy carbon electrode

Before modification of the surface, glassy carbon electrode (GCE, dia. 3 mm) was polished with 1 μm and 0.05 μm alumina slurries sequentially, and then rinsed with DI water. Afterwards, the electrode was cleaned by ultra-sonic bath for 5 min in acetone, ethanol and DI water in sequence, and then dried at room temperature. The loading of IrO_2-Au NCs on the glassy carbon electrode was first optimized using cyclic voltammetry in 0.1 M NaOH and in 0.01 M PBS buffer. 7 mg/mL of IrO_2-Au NCs with a fixed loading volume of 8 μL shows the best CV response, thus being used for subsequent experiments. To prepare 7 mg/mL IrO_2-Au NCs suspension, 7 mg of calcined IrO_2-Au NCs sample was suspended in 1.0 ml ethanol and then subject to 30 min of ultra-sonication. Afterwards, 8 μL IrO_2-Au NCs/ethanol suspension was drop-cast onto the pre-cleaned glassy carbon electrodes. After solvent evaporation, 5 μL of Nafion solution (1wt% in ethanol) was further drop-cast onto the top of IrO_2-Au NCs and dried in air to entrap the nanoclusters. The as-prepared electrode is denoted as Nafion/IrO_2-Au NCs/GCE. Nafion-coated glassy carbon electrode (Nafion/GCE) was also prepared as a control electrode following the same procedure. Before use, each electrode was submerged into DI water for an appropriate time to allow Nafion membrane to swell. All experiments were repeated for at least 3 times to ensure the reproducibility.

2.4 Apparatus and electrochemical measurements

A JEOL 6335F field-emission scanning electron microscope (SEM) was used to examine the morphology and the size of the as-electrospun precursory nanofibers and IrO_2-Au NCs. Transmission electron microscopic (TEM) images, high angle annular dark field-scanning transmission electron microscopic (HAADF-STEM) images, energy dispersive X-ray (EDX) elemental mapping data, and selected area electron diffraction (SAED) patterns were acquired using a Thermo Fisher Scientific -Talos microscope operated at an accelerating voltage of 200 kV. The X-ray powder diffraction patterns (XRD) were obtained with a Rigaku UltimaIV instrument with Cu Kα radiation (=0.154056 nm) operating at 40 kV and 45 mA beam current. Raman spectra were recorded at ambient temperature on a Reinshaw Ramanscope Micro-Raman with 514 nm wavelength lasers. Cyclic voltammetry (CV), amperometry and open circuit potential measurements were performed on a CHI 601C Electrochemical Workstation (CH Instruments, USA). All experiments were conducted using a standard three-electrode electrochemical cell, consisting of a working electrode (GCE, dia. 3 mm), an Ag/AgCl reference electrode, and a platinum counter electrode (dia. 3 mm). For amperometric glucose detection, all signals were recorded after current decayed to a steady-state value and a stirrer was used to provide convective mixing. For pH sensing, the pH-adjustable buffer was prepared using a recipe from a previous report.[20] Briefly, pH 3.0-9.0 solutions were universal buffers containing 10 mM potassium hydrogen phthalate, 10 mM phosphate, and 10 mM Tris, while pH 10.0 and 13.0 solutions contained 50 mM sodium carbonate and 10 mM borax and 140 mM of NaCl. The pH adjustment was realized by addition of 1 M HNO_3 or 1 M NaOH.

3. Results and discussion

3.1 Morphology and composition of IrO_2-Au NCs

Fig. 1A shows the typical morphology of the precursory $IrCl_4$-$HAuCl_4$/PVP nanofibers. One can see that the precursory nanofibers possessed smooth surface and the diameter of the precursory nanofibers is 130 ± 23 nm ($IrCl_4$/$HAuCl_4$/PVP nanofibers). After degradation of PVP and decomposition of $IrCl_4$ and $HAuCl_4$ at high temperature, a nanocluster morphology was formed (Fig. 1B) due to the migration of iridium oxide and Au element.

The as-prepared nanoclusters in ethanol suspension were subjected to 30 min of ultrasonication before TEM characterization. TEM image (Fig. 2) also reveals that the IrO_2-Au shows nanocluster structure, in good agreement with Fig. 1B. Furthermore, the element mapping of Ir, Au, and O in Fig. 2 indicates that the element gold is uniformly distributed into the backbone of iridium and oxygen. The d-spacing values in Fig. 3B were measured to be 0.314 nm and 0.231 nm, 0.204 nm, which can be attributed to (1 1 0) planes of IrO_2 and (1 1 1) and (2 0 0) planes of elemental Au. The SAED patterns shown in Fig. 3C clearly display several rings, which can be indexed to the planes of (1 1 0), (1 0 1), (2 1 1), (4 0 0) of IrO_2 fluorite-like structure and (1 1 1) and (2 2 0) planes of elemental Au. These studies indicate that Au was successfully doped into IrO_2.

In order to monitor the composition change of $IrCl_4$/$HAuCl_4$/PVP precursor before and after annealing process, Fourier-Transform Infrared spectroscopy (FT-IR) was applied to analyze the samples. One can see that the transmission bands associated with PVP at ca. 1640 cm^{-1}, 1420

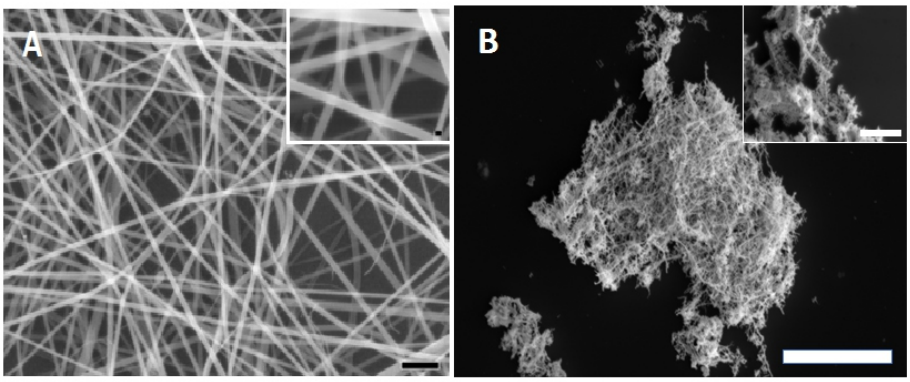

Fig. 1 (A) SEM image of $IrCl_4$/$HAuCl_4$/PVP nanofibers (Scale bar: 1 μm and 100 nm for inset). (B) SEM image of annealed IrO_2-Au nanoclusters. (Scale bar: 10 μm and 2 μm for inset).

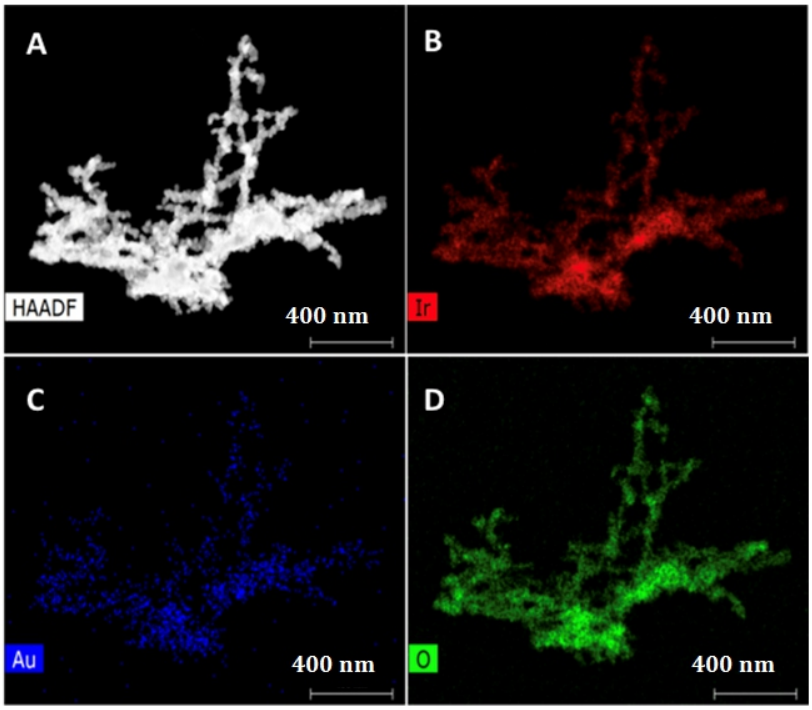

Fig. 2 TEM metal mapping to the gold-doped iridium oxide nanoclusters with HAADF (A), Ir mapping (B), Au mapping (C), and O mapping (D), respectively.

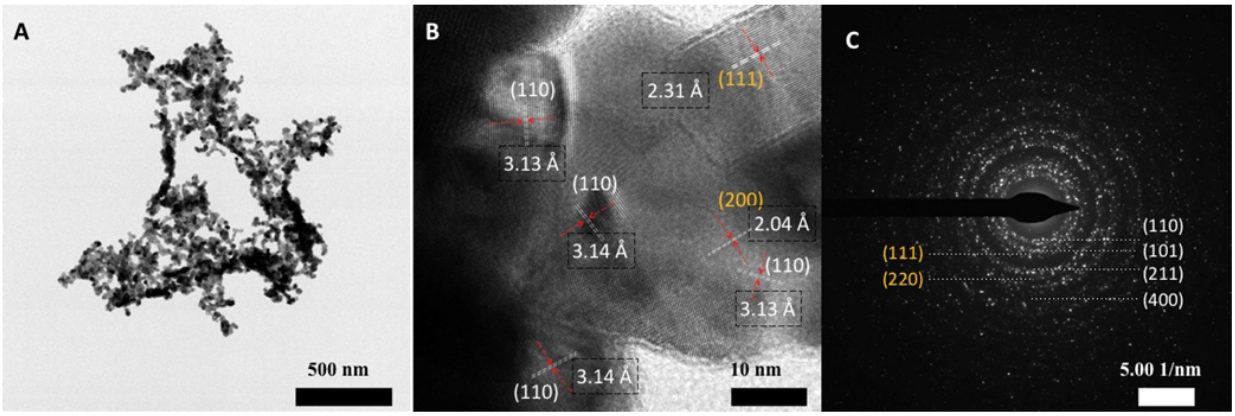

Fig. 3 (A) TEM image of IrO_2-Au NCs (Scale bar 500 nm). (B) HRTEM image of IrO_2-Au NCs (Scale bar 10 nm). The corresponding miller indices are labeled in yellow for Au and white for iridium oxide. (C) The SAED pattern (Scale bar 5.00 1/nm).

cm^{-1}, and 1290 cm^{-1} disappeared after calcination, shown in Fig. 4, indicating complete degradation of PVP.

To investigate phase purity of the as-synthesized gold-doped IrO_2 nanoclusters, IrO_2 nanoclusters, and gold particles, X-ray powder diffraction was applied for analysis and the results are presented in Fig. 5. The diffractions at 2θ=38.09°, 44.29°, 64.50°, 77.49° and 81.68° (not shown) were measured and recorded in the calcined Au particles, and they were fit into the miller index of (111), (200), (220), (311), and (222) (JCPDS Card File No. 03-065-2870). The reflections at 2θ=27.85°, 34.51°, 39.80°, 40.44°, 53.79°, 57.77°, 58.21°, 65.39°, 65.91°, 69.06°, and 73.14° were detected in the as-prepared IrO_2 NCs. All peaks fit well with IrO_2 (110), (101), (200), (111), (211), (220), (002), (310), (112), (301), and (202) (JCPDS Card File No. 15-0870), which indicate the typical cubic fluorite-like structure of IrO_2. Typical Raman spectra of the as-prepared IrO_2-Au NCs and the precursory $IrCl_4$/$HAuCl_4$/PVP nanofibers are shown in Fig. 6. There is no obvious peak observed for precursory nanofibers. However, there are two major peaks (at 550 and 718 cm^{-1}) and one minor shoulder peak (at 743 cm^{-1}) for the IrO_2-Au NCs. Those peaks can be assigned to E_g, B_{2g} and A_{1g} modes of the crystalline IrO_2, further indicating the formation of IrO_2. Moreover, no carbon trace was observed in calcined IrO_2–Au NCs, which was corroborated by the lack of carbon's G-band at ~1600 cm^{-1}.

3.2 Electrochemical behavior of the IrO_2-Au NCs modified GCE (Nafion/IrO_2-Au NCs/GCE) toward both glucose and pH monitoring

3.2.1 Glucose sensing

Being attacked by hydroxide ions, iridium oxide has been reported to form different oxidation valences, thus endowing the electrochemical redox capability. In this study, 0.1 M NaOH and 0.01 M PBS buffer were used as electrolytes to scrutinize the performance of the as-prepared Nafion/IrO_2-Au NCs/GCE for non-enzymatic glucose sensing. The CVs (scanning from -0.5 V to +0.8 V vs. Ag/AgCl) of the Nafion/GCE (Fig. 7A) and Nafion/IrO_2-Au NCs/GCE in the absence and presence of 5 mM and 10 mM of glucose were first investigated in alkaline solution (0.1 M NaOH) and then 0.01 M PBS buffer, respectively. In the absence and presence of glucose, there was no

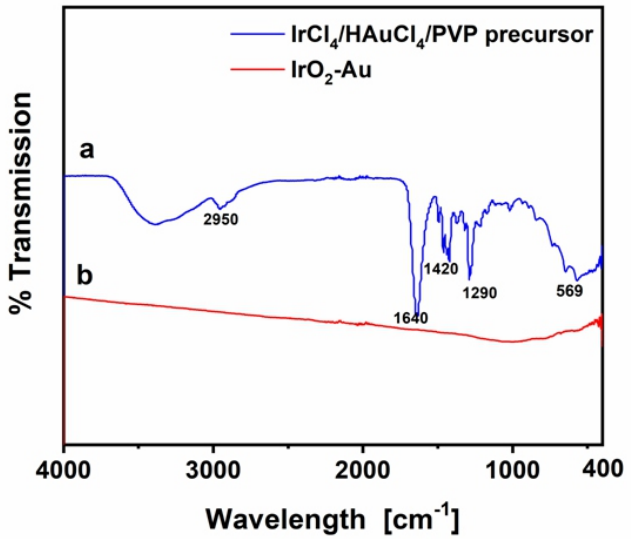

Fig. 4 The Fourier-transform infrared spectra of $IrCl_4$/$HAuCl_4$/PVP precursory nanofibers and the calcined IrO_2-Au powder, respectively.

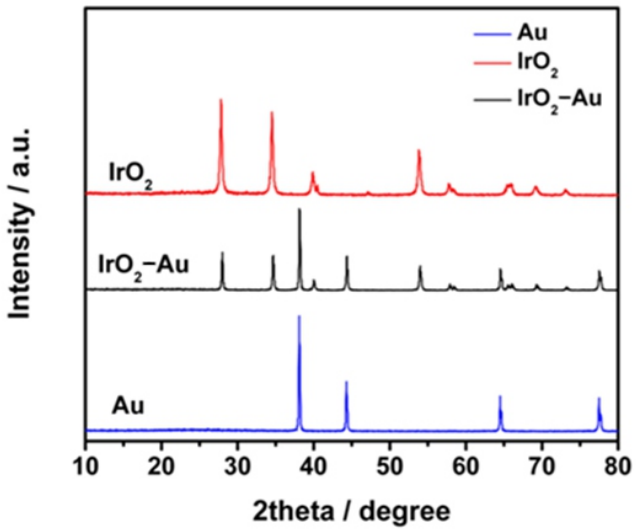

Fig. 5 The X-ray powder diffraction (XRD) analyses of Au (blue line), IrO_2 (red line), and IrO_2-Au (black line) from calcined $HAuCl_4$/PVP, $IrCl_4$/PVP, and $IrCl_4$/$HAuCl_4$/PVP precursory nanofibers, respectively.

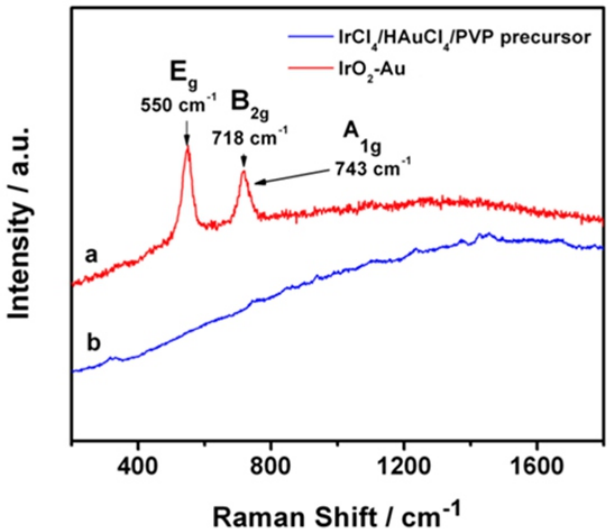

Fig. 6 The Raman spectra of calcined IrO_2-Au nanoclusters (a) and precursory $IrCl_4$/$HAuCl_4$/PVP nanofibers (b), respectively.

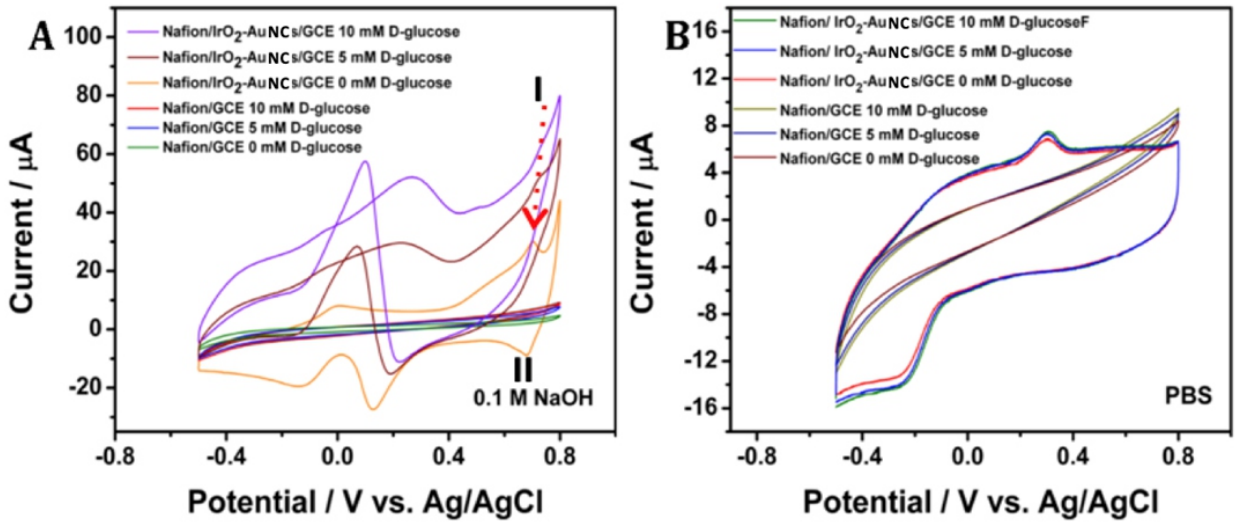

Fig. 7 (A) Cyclic voltammetry response of Nafion/GCE and Nafion/IrO_2-Au NCs/GCE in the absence and presence of 5 mM and 10 mM glucose in 0.1 M NaOH electrolyte. (B) Cyclic voltammetry response of Nafion/GCE and Nafion/IrO_2-Au NCs/GCE in the absence and presence of 5 mM and 10 mM glucose in 0.01 M PBS buffer.

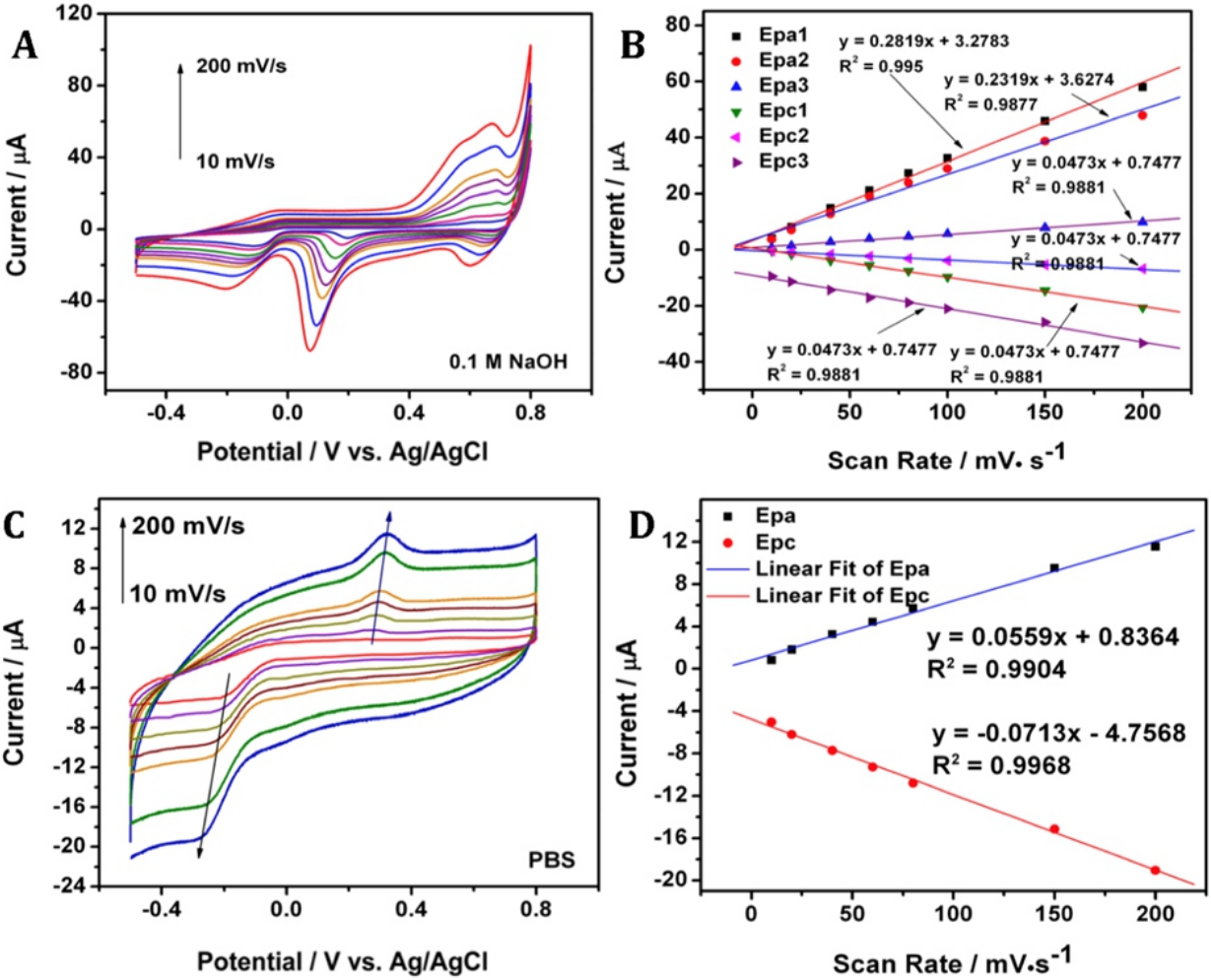

Fig. 8 Cyclic voltammetry response of Nafion/IrO_2-Au NCs/GCE in the absence of glucose at different scanning rate of 10 mV/s, 20 mV/s, 40 mV/s, 60 mV/s, 80 mV/s, 100 mV/s, 150 mV/s, 200 mV/s in 0.1 M NaOH electrolyte (A) and at different scanning rate of 10 mV/s, 20 mV/s, 40 mV/s, 60 mV/s, 80 mV/s, 150 mV/s, 200 mV/s in 0.01 M PBS buffer (C),, and their corresponding plot of peak current vs. scan rate in 0.1 M NaOH (B) and in 0.01 M PBS (D).

obvious peak observed on the Nafion/GCE, indicating negligible catalytic character towards glucose. The one for the Nafion/IrO_2-Au NCs/GCE shows both typical characteristic for a gold electrode (gold oxide formation and reduction) and a typical characteristic for an iridium oxide electrode (iridium oxidation (I) and reduction (II)) in the electrolyte of 0.1 M NaOH. The result was in a good agreement with literature reports for gold[21-30] or iridium oxide.[17] Therefore, IrO_2-Au NCs in Nafion/IrO_2-Au NCs/GCE was responsible for the indication of glucose oxidation in alkaline environment. With the increase of glucose concentration, the peak current at ca. +0.05 V increased accordingly and far more prominent than the characteristic peak of iridium oxide at ca. +0.67 V. Therefore, we chose to measure the glucose concentration by using the characteristic peak of gold because of its low operational potential and more pronounced response towards glucose. On the contrary, in the neutral solution of 0.01 M PBS, the responses of both Nafion/GCE and Nafion/IrO_2-Au NCs/GCE towards the absence and presence of glucose did not display obvious difference, as shown in Fig. 7B, indicating the necessity of alkaline environment for non-enzymatic glucose oxidation. Therefore, glucose sensing was pursued only in alkaline environment.

Furthermore, Fig. 8 demonstrates the effect of the scan rate on the oxidation and reduction peak currents in the electrolyte of 0.1 M NaOH and 0.01 M PBS buffer, respectively. One can observe that the oxidation and reduction peak current linearly increased with the scan rate from 10 mV/s to 200 mV/s (Fig. 8B and 8D), indicating the typical surface-controlled electrochemical process for Nafion/IrO_2-Au NCs/GCE in both electrolytes.

As the oxidation peak current of Nafion/IrO_2-Au NCs/GCE at ca. +0.05 V in 0.1 M NaOH increases proportionally with glucose concentration, amperometric glucose detection using Nafion/IrO_2-Au NCs/GCE was conducted at an applied potential of +0.05 V (vs. Ag/AgCl) in the electrolyte of 0.1 M NaOH. Fig. 9A shows the typical amperometric responses of the developed sensor to successive injection of glucose in 0.1 M NaOH solution. A well-defined, stable and fast

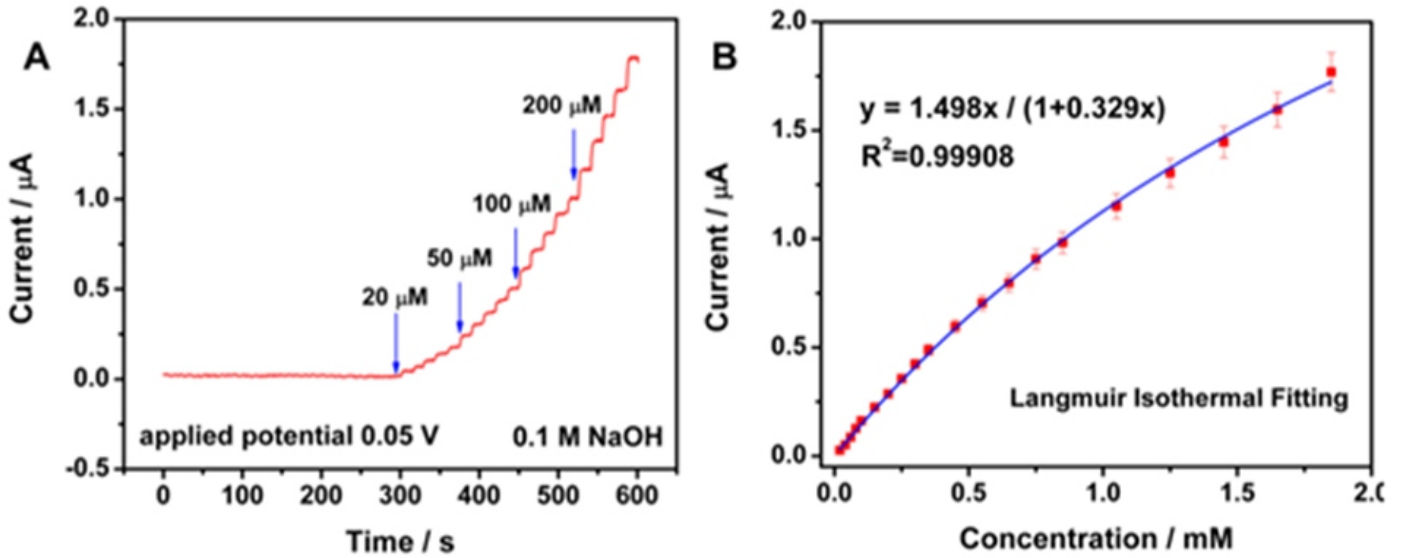

Fig. 9 Typical Amperometric response of Nafion/IrO_2-Au NCs/GCE electrode toward glucose addition in 0.1 M NaOH at +0.05 V (vs. Ag/AgCl) (A) and the corresponding calibration curves (B).

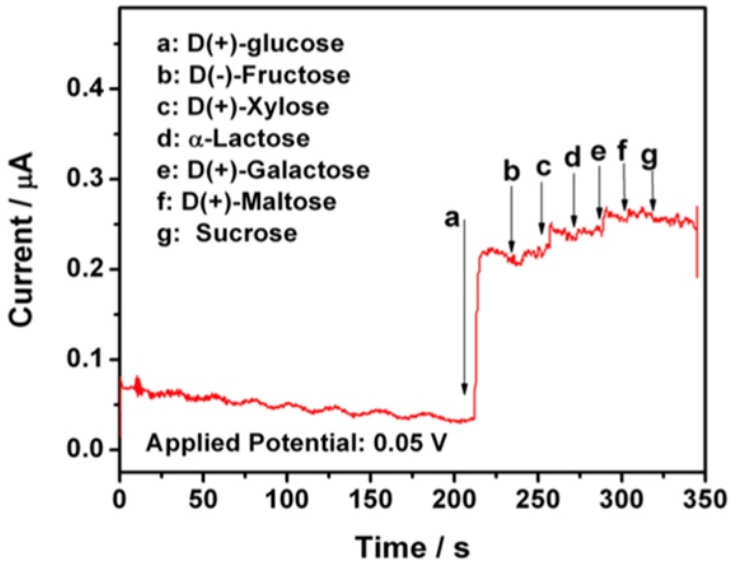

Fig. 10 Amperometric response of Nafion/IrO_2-Au NCs/GCE towards 100 μM of glucose, and 10 μM of fructose, xylose, α-lactose, galactose, maltose, and sucrose, respectively.

amperometric response within 5 s can be observed on the Nafion/IrO_2-Au NCs/GCE. With the successive addition of glucose, the Nafion/IrO_2-Au NCs/GCE generated a stepwise amperometric response. The corresponding calibration curve of the current vs. glucose concentration is plotted and presented as Fig. 9B. The electrochemical oxidation of glucose on IrO_2–Au NCs is a surface catalytic reaction, which is typically well described by Langmuir isothermal theory in our previous study.[8] Therefore, Langmuir isothermal theory was adopted to fit the calibration curve (Fig. 9B) with good fitting results (a correlation coefficient of 0.999).

$$I(\mu A) = \frac{1.498 C_{glucose}(mM)}{1 + 0.329 C_{glucose}(mM)}$$

According to the surface area of GCE, the sensitivity and the limit of detection (S/N=3) were calculated to be 21.20 μA mM^{-1} cm^{-2} and 2.93 μM, respectively.

3.2.1.2 Selectivity of Nafion/IrO_2-Au NCs/GCE

The selectivity of the Nafion/IrO_2-Au NCs/GCE in 0.1 M NaOH solution was also investigated against normally co-existed interfering species with glucose such as fructose, xylose, lactose, galactose, maltose, sucrose, dopamine (DA), 4-acetoamenophen (4-AP), uric acid (UA), and ascorbic acid (AA). As the concentration of glucose in blood is typically at least 10-fold higher than those of common interferences,[31] the amperometric signal of 100 μM glucose on the Nafion/IrO_2-Au NCs/GCE were compared with those of 10 μM fructose, xylose, lactose, galactose, maltose, sucrose, 4-AP, UA, and AA. Wang, J. *et al.*[32] also reported the similar selectivity test for the glucose concentration towards interferences. Fig. 10 shows the current vs. time curve of the Nafion/IrO_2–Au NCs/GCE toward the sequential injection of glucose and interfering sugars in the electrolyte of 0.1 M NaOH. As shown, only xylose and galactose result in a very minor interference. In addition, the response to 10 μM 4-AP, UA, and AA is 3%, 16% and 25% of the response to 100 μM glucose, respectively. This study indicates the reasonable selectivity of the developed sensor against most of co-existing interference compounds in glucose detection.

3.2.2 pH sensing using the Nafion/IrO_2–Au NCs/GCE

In aqueous condition, by recording electromotive force (EMF) in varied pH buffer, Nernst-constant can be calculated using a calibrated curve. Since the report of both anodically oxidized iridium oxide (AOIRF) and cathodically oxidized iridium oxide (COIRF),[33] iridium oxide has been extensively exploited in solid-state pH sensing. Typically, the redox intercalation equilibrium can be found in different oxidation states of IrO_x, which is attributed to its pH sensing mechanism.[34-37] To test the pH

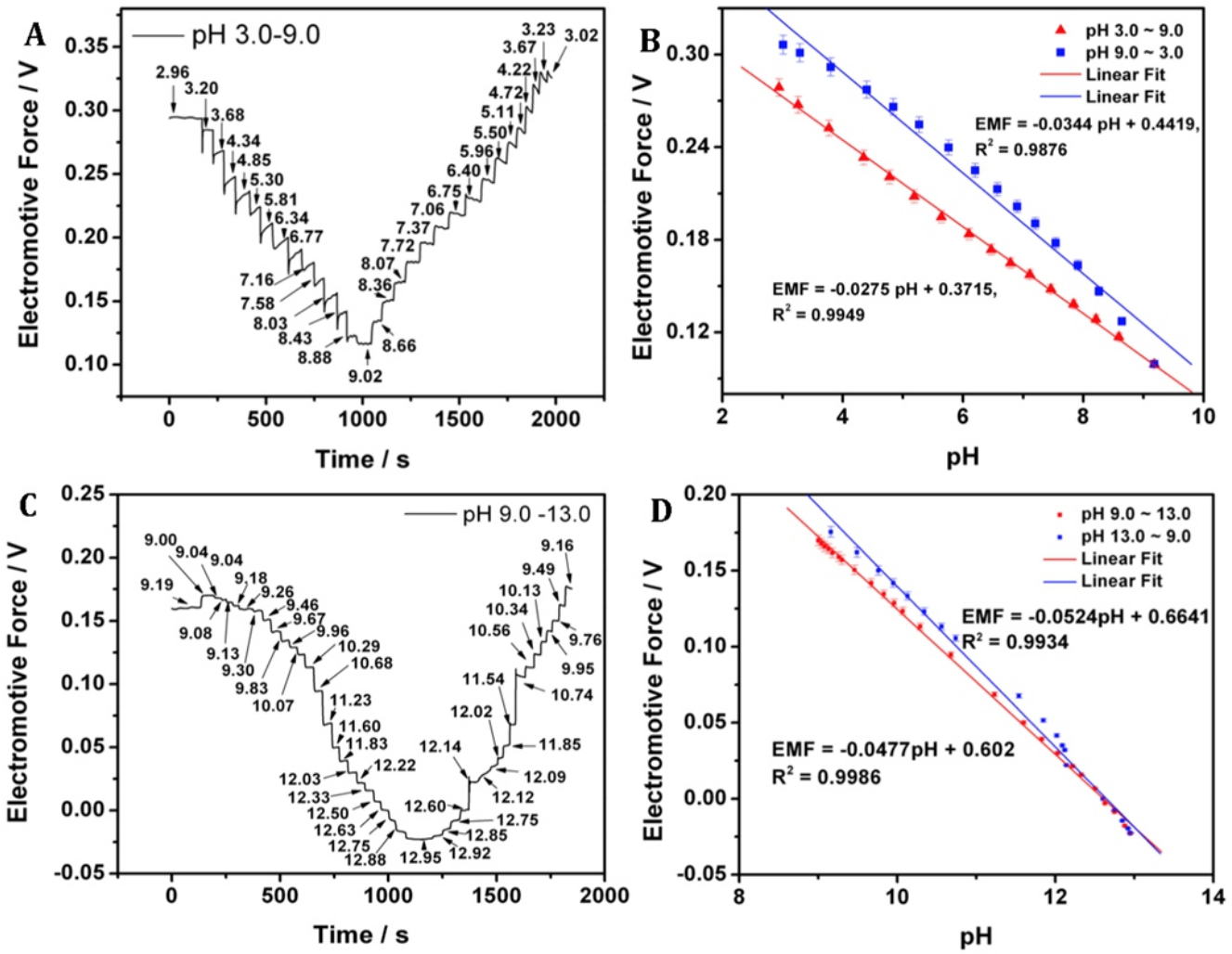

Fig. 11 pH titration response of Nafion/IrO_2-Au NCs/GCE in the range of pH 3.0 to 9.0 (A) and pH 9.0 to 13.0 (C) and the corresponding EMF vs. pH plots (B and D).

sensitivity of the developed Nafion/IrO_2-Au NCs/GCE, pH titration experiments were conducted in different pH ranges. As a comparison, a commercial pH meter was used to record the pH variation in the same solution simultaneously. The corresponding EMF value was recorded in real-time format and shown in Fig. 11A and 11C. We observed that the Nafion/IrO_2-Au NCs/GCE responded to pH variation rapidly and the relative stable potential were typically acquired within 10 seconds, which is comparable with the stabilizing time for a commercial pH meter. The calculated Nernst constants are 27.50 mV/pH (titration from pH 3 to pH 9), 34.40 mV/pH (titration from pH 9 to pH 3), 47.70 mV/pH (titration from pH 9 to pH 13) and 52.40 mV/pH (titration from pH 13 to pH 9). Hysteresis was observed during titration experiment, which reflects the deviation of the open circuit potential for the same pH value. It could be ascribed to several factors, including different thermodynamic equilibrium formed at the same pH value, different hydration degree of gold-doped iridium oxide nanoclusters, etc. The slopes in Fig. 11B and D showed sub-Nernst constant at room temperature (25 °C) compared with the theoretical value of 59 mV. For the clarification of the Nafion membrane effect in pH titration experiment, Nafion/GCE was used in the same procedures. The corresponding Nernst constants are 5.8 mV/pH and 5.9 mV/pH during titration in the range of pH 3 to 9 and pH 9 to 3, respectively, and negligible sensitivity towards pH change in pH 9 to 13 and pH 13 to 9 (data not shown), which indicate that the effect of Nafion on pH sensing of Nafion/IrO_2-Au NCs/GCE is minor.

4. Conclusions

In summary, a novel dual electrochemical sensor based on IrO_2-Au NCs modified glassy carbon electrode was developed. Due to pH sensitivity of iridium oxide and glucose oxidation capability of gold in IrO_2-Au NCs, the developed sensor was applied for both non-enzymatic glucose sensing in alkaline environment and pH monitoring. The results show that the IrO_2 is responsible for the observed pH sensing capability, while Au is attributed to glucose detection at a low applied potential in alkaline environment. All these features indicate that the high-temperature annealed IrO_2-Au NCs are a promising multifunctional sensing material for the development of an integrated solid-state pH sensor and non-enzymatic glucose sensor.

Acknowledgments

We greatly appreciate the funding from EPA Challenging Grant and USGS. HML also thank the support from GE Fellowship. This work was supported in part by the award of a Thermo Fisher Scientific Graduate Fellowship to XW. The TEM studies were performed using the facilities in the UConn/Thermo Fisher Scientific Center for Advanced Microscopy and Materials Analysis (CAMMA).

Conflict of Interest

None.

References

1. J. C. Chou and L. P. Liao, *Thin Solid Films,* 2005, **476** (1), 157-161.
2. H. Chen, Y. S. Rim, I. C. Wang, C. Li, B. Zhu, M. Sun, M. S. Goorsky, X. He and Y. Yang , *ACS nano,* 2017, **11** (5), 4710-4718.
3. P. Batista and M. Mulato, *Appl. Phys. Lett.,* 2005, **87** (14), 143508.
4. B. Liu, Y. Su and S. Chen, *Int. J. Electron. Theor. Exp.,* 1989, **67** (1), 59-63.
5. W. Lv, C. H. You, S. Wu, B. Li, Z. P. Zhu, M. Wang, Q. H. Yang and F. Kang, *Carbon,* 2012, **50** (9), 3233-3239.
6. Y. Cheng, P. Xiong, C. S. Yun, G. Strouse, J. Zheng, R. Yang and Z. Wang, *Nano lett.,* 2008, **8** (12), 4179-4184.
7. A. Ramsing, J. Janata, J. Růžička and M. Levy, *Anal. Chim. Acta,* 1980, **118** (1), 45-52.
8. Y. Ding, Y. Wang, L. Su, M. Bellagamba, H. Zhang and Y. Lei, *Biosens. Bioelectron.,* 2010, **26** (2), 542-548.
9. C. W. Kung, C. Y. Lin, Y. H. Lai, R. Vittal and K. C. Ho, *Biosens. Bioelectron.,* 2011, **27** (1), 125-131.
10. Q. Dong, X. Wang, W. S. Willis, D. Song, Y. Huang, J. Zhao, B. Li and Y. Lei, *Electroanal.,* 2019.
11. X. Y. Lang, H. Y. Fu, C. Hou, G. F. Han, P. Yang, Y. B. Liu and Q. Jiang, *Nat. commun.,* 2013, **4**, 2169.
12. F. Cao, S. Guo, H. Ma, D. Shan, S. Yang and J. Gong, *Biosens. Bioelectron.,* 2011, **26** (5), 2756-2760.
13. Y. Ding, Y. Liu, J. Parisi, L. Zhang and Y. Lei, *Biosens. Bioelectron.,* 2011, **28** (1), 393-398.
14. J. Song, L. Xu, C. Zhou, R. Xing, Q. Dai, D. Liu and H. Song, *ACS Appl. Materi. Int.,* 2013, **5** (24), 12928-12934.
15. A. Molazemhosseini, L. Magagnin, P. Vena and C. C. Liu, *J. Electroanal. Chem.,* 2017, **789**, 50-57.
16. M. Long, L. Tan and A. D. Tang, *Adv.Mater. Res*., 2014, 3-8.
17. Q. Dong, D. Song, Y. Huang, Z. Xu, J. H. Chapman, W. S. Willis, B. Li and Y. Lei, *Electrochim. Acta,* 2018, **281**, 117-126.
18. T. M. Cheng, T. K. Huang, H. K. Lin, S. P. Tung, Y. L. Chen, C. Y. Lee and H. T. Chiu, *ACS Appl.Mater. Int.,* 2010, **2** (10), 2773-2780.
19. S. Park, S. Park, R. A. Jeong, H. Boo, J. Park, H. C. Kim and T. D. Chung, *Biosens. Bioelectron.,* 2012, **31** (1), 284-291.
20. S. A. Marzouk, *Analy. Chem..,* 2003, **75** (6), 1258-1266.
21. G. Chang, H. Shu, K. Ji, M. Oyama, X. Liu and Y. He, *Appl. Surf. Sci.,* 2014, **288**, 524-529.
22. Y. Gu, R. Yuan, X. Yan, C. Li, W. Liu, R. Chen, L. Tang, B. Zheng, Y. Li and Z. Zhang, *Analy. Chim.acta,* 2015, **889**, 113-122.
23. C. W. Hsu, F. C. Su, P. Y. Peng, H. T. Young, S. Liao and G. J. Wang, *Sensor. Actuat. B-Chem.,* 2016, **230**, 559-565.
24. C. Li, Y. Su, X. Lv, H. Xia, H. Shi, X. Yang, J. Zhang and Y. Wang, *Biosens. Bioelectron.,* 2012, **38** (1), 402-406.
25. A. Liu, Q. Ren, T. Xu, M. Yuan and W. Tang, *Sensor. Actuat. B-Chem.,* 2012, **162** (1), 135-142.
26. L. Rassaei and F. Marken, *Anal. Chem..,* 2010, **82** (17), 7063-7067.
27. R. Sedghi and Z. Pezeshkian, *Sensor. Actuat. B-Chem.,* 2015, **219**, 119-124.
28. T. D. Thanh, J. Balamurugan, S. H. Lee, N. H. Kim and J. H. Lee, *Biosens. Bioelectron.,* 2016, **81**, 259-267.
29. C. Wang, X. G. Nie, Y. Shi, Y. Zhou, J. J. Xu, X. H. Xia and H. Y. Chen, *ACS nano,* 2017.
30. H. Zhu, X. Lu, M. Li, Y. Shao and Z. Zhu, *Talanta,* 2009, **79** (5), 1446-1453.
31. Q. Dong, Y. Huang, D. Song, H. Wu, F. Cao and Y. Lei, *Biosens. Bioelectron.,* 2018, **112**, 136-142.
32. J. Wang, L. Xu, Y. Lu, K. Sheng, W. Liu, C. Chen, Y. Li, B. Dong and H. Song, *Anal. Chem.,* 2016, **88** (24), 12346-12353.
33. K. Yamanaka, *Jap.J.Appl. Phys.,* 1989, **28** (4R), 632.
34. Q. Zeng, K. Xia, B. Sun, Y. Yin, T.Wu and M. S. Humayun, *Electrochim. Acta,* 2017, **237**, 152-159.
35. J. Juodkazytė, B. Šebeka, I. Valsiunas and K. Juodkazis, *Electroanal.,* 2005, **17** (11), 947-952.
36. P. J. Kinlen, J. E. Heider and D. E. Hubbard, *Sensor. Actuat. B-Chem.,* 1994, **22** (1), 13-25.
37. H. Leiva, R. Kershaw, K. Dwight and A. Wold, *Mater. Res. Bull.,* 1982, **17** (12), 1539-1544.